Dynamic modelling, simulation and economic evaluation of two CHO cell-based production modes towards developing biopharmaceutical manufacturing processes

Dynamic modelling, simulation and economic evaluation of two CHO cell-based production modes towards developing biopharmaceutical manufacturing processes

Haruku Shirahata[a], Samir Diab[b], Hirokazu Sugiyama[a], Dimitrios I. Gerogiorgis[b*]

[a] Department of Chemical System Engineering, School of Engineering, University of Tokyo, Hongo Campus, Tokyo 113-8656, Japan

[b] Institute for Materials and Processes (IMP), School of Engineering, University of Edinburgh, The Kings Buildings, Edinburgh, EH9 3FB, United Kingdom

**Corresponding Author*: D.Gerogiorgis@ed.ac.uk (*+44 131 6517072*)

ABSTRACT

Chinese Hamster Ovary (CHO) cells are widely used in fermentation towards biopharmaceutical manufacturing. The present paper presents dynamic mathematical models of two different CHO culture modes: one batch mode for the production of interferon, and one perfusion mode for the production of a monoclonal antibody (mAb). The dynamic models have been used for simulating cell, substrate, by-product and product concentration trajectories, which have been compared against previously published experimental results. A sensitivity analysis of both models has been conducted, in order to analyse the relative importance of operating parameters towards biopharmaceutical process design. An economic analysis has also been subsequently performed: time and net present cost for given target capacities have been evaluated, using the validated dynamic models for the batch and perfusion modes. Economic trends have been discussed for variable initial concentration of viable CHO cells to be used in bioreactors: the latter has been recognized as the most sensitive model parameter for both culture modes.

Keywords: Monoclonal antibody (mAb), perfusion culture; Monod equation; process design; economic evaluation; biopharmaceutical manufacturing.

1. Introduction

1.1 Fermentation process of biopharmaceutical manufacturing

The biopharmaceuticals market is growing rapidly with an approximate revenue of $163 billion (Otto et al., 2014). The growth rate of the market is around 8%, twice that of conventional pharmaceuticals. For industrial-scale manufacturing, biopharmaceuticals are typically produced in two main stages: drug substance manufacturing for synthesizing Active Pharmaceutical Ingredients (APIs) and drug product (DP) manufacturing formulating the APIs in, e.g., vials or syringes. A biopharmaceutical manufacturing process comprises the *upstream process* for fermentation and the *downstream process* for harvesting and purification. Among the biopharmaceutical products, monoclonal antibodies (mAbs) are dominant, representing approximately half of the total sales of biopharmaceuticals (Ecker et al., 2015). Monoclonal antibodies are produced by fermenting mammalian cells; Chinese Hamster Ovary (CHO) cells are commonly used to produce complex proteins.

Production of mAbs by means of employing CHO cell cultures is widely implemented in industrial manufacturing with different culture modes: batch, fed-batch, and perfusion cultures (Bielser et al., 2018). *Batch and fed-batch modes* feed substrate only once or continuously to keep nutrient concentration constant, respectively, being dominant conventional technologies for mAb manufacturing. The *fed-batch mode* is an established industrial standard for mAb production, despite the problem of waste product accumulation, which inhibits cell growth. In contrast to these two methods, an emerging trend in continuous biomanufacturing is the *perfusion mode*, a technology

whose deployment in continuous manufacturing has become more widespread in recent years (Fisher et al., 2019), which retains cells in the bioreactor while simultaneously harvesting products. Industrial corporations are now moving towards adopting perfusion modes for numerous production lines, due to the higher productivity that can be achieved in comparison to the foregoing conventional methods (Langer and Rader, 2014).

1.2 Process performance analysis

Experiments to measure the profile of cell densities, substrate concentration and product concentration have been published for both antibody (Lee et al., 2005) and β-interferon (Sunley et al., 2008; Tharmalingam et al., 2008) production in batch mode cultures. Badsha et al. (2015) conducted a metabolic analysis of CHO cells in batch mode for antibody production under different stress conditions, with NaCl and trehalose addition to suppress cell growth. In the fed-batch mode, an investigation for selecting cell lines with high process performance has been recently published (Rouiller et al., 2016), while other studies have analysed metabolic fluxes for nutrient consumption and product formation (Ahn and Antoniewicz, 2011; Templeton et al., 2013). Concentrated fed-batch cell cultures can be implemented even with limited volume capacity when using improved cell culture titer (Yang et al., 2016). Process performance by means of measuring oxygen uptake rate (OUR) has also been measured for fed-batch mode (Huang et al., 2010). The effect of process scale-up on bioreactors up to 5,000 L has also been investigated by considering the OUR metric (Xing et al., 2009).

Experimental studies have also been conducted and published for perfusion mode (Dowd et al., 2003). The latter is expected to yield higher cell density than conventional culture modes, and a recent investigation of culture conditions reports a yield as high as 250×10^6 cells/ mL (Zhang et al., 2015). Process performance has been similarly tested for different bioreactor configurations using different filters, e.g. conventional tangential flow (TFF) and alternating tangential flow filtration (ATFF) (Clincke et al., 2013a, 2013b; Karst et al., 2016). There are other investigations of perfusion mode production, e.g., process performance analyses when integrating the fermentation unit with subsequent downstream capture processes (Karst et al., 2017b; Steinebach et al., 2017). A new culture mode has been recently reported; therein, perfusion and fed-batch modes are combined in order to avoid lactate accumulation and to increase productivity (Hiller et al., 2017).

Combinations of these three different culture modes (batch, fed-batch, and perfusion mode) have also been investigated in recent publications. Individual experiments for the three different culture modes have been conducted (Hu et al., 2011), and modelling CHO metabolism in order to elucidate its effect on cell growth, productivity and glycosylation has been reviewed (Galleguillos et al., 2017). Sokolov et al. (2017) applied the experimental results of a fed-batch process to identify preferable process conditions for early process development. Beyond perfusion mode, a single-use technology using disposable resin-based equipment has been invented to replace the limitations of conventional multi-use technologies, which rely on expensive stainless-steel vessels and facilities. The technology can reduce the complexity and cost due to change-over operations for multi-product plants; nevertheless, concerns about leachable chemical compounds which can migrate from resin containment materials into drug solutions are serious, and such effects on CHO cell growth inhibition are reported (Kelly et al., 2016).

1.3 Modelling approach

Modelling of fermentation kinetics have been mainly conducted for non-CHO cells. For example, modelling and optimisation have been conducted for fermentation of *E. coli* with a comparison of different algorithms (Rocha et al., 2014). A mechanistic model has been applied to predict and monitor process performance of fermentation of filamentous fungi (Mears et al., 2017) and lactic acid bacteria (Spann et al., 2018). Dynamic modelling has been conducted in beer fermentation processes, and the models were applied to sensitivity analysis and multi-objective process optimisation (Rodman and Gerogiorgis, 2016, 2017; Rodman et al., 2018).

As for CHO fermentation, kinetic models have been developed for batch mode and validated using experimental results obtained from a packed-bed bioreactor (Shakibaie et al., 2011). Model development for the fed-batch mode of CHO cells has been investigated by applying the Markov Chain Monte Carlo method for fed-batch mode (Xing et al., 2010).

Published studies have also used plant data to design biopharmaceutical processes relying on fermentation. For example, different (fed-batch and perfusion) culture modes have been evaluated regarding the cost of goods by integrating fermentation and downstream processes (Klutz et al., 2016). Bunnak et al. (2016) evaluated the life-cycle cost of goods of different (fed-batch and perfusion) culture modes, along with an evaluation on the environmental effects such as water consumption, energy input and CO_2 emission. In both lab-scale and commercial mAb manufacturing, integrated continuous processes have been evaluated with respect to their economic, operational, and environmental feasibility (Pollock et al., 2017). The foregoing process analysis methodologies can be implemented towards systematic biopharmaceutical process design and decision-making regarding investment in new technologies, but have exclusively relied on experiments and plant data to evaluate economic and environmental impact; cell growth and production kinetic models have not been hitherto considered as fundamental building blocks of technoeconomic analyses of biopharmaceutical manufacturing concepts, hence this contribution aims to offer a new perspective on combining models and data to this key end.

1.4 Summary and objectives

The key (batch and fed-batch) culture modes for producing biopharmaceuticals have different process performance and variable concerns regarding productivity, resource usage, culture duration and economic impact. To select and design a culture mode quantitatively, kinetic modelling is a useful, versatile tool in order to describe and assess process performance. Previous studies mainly focus on experimental approaches to improve culture conditions, or mathematical models developed mainly to replicate the physical phenomena of fermentation. The approach of dynamic modelling with kinetic parameters has yet to be applied to employ economic evaluation toward design of CHO fermentation modes; therein lies the novelty of this work.

The objective of this paper is to implement mathematical models incorporating kinetics of CHO cell fermentation for different types of cultures for evaluation of different process design spaces. The batch and perfusion modes are the two options selected in the present study. Kinetic models are firstly described and compared with experimental results to achieve validation against two recent publications, which present experimental results for CHO cell fermentation, one for each culture mode. Next, the developed models have been used for a parametric sensitivity analysis, where the effects of parameters on dynamic states have been investigated. Finally, an economic evaluation of both culture modes is conducted by perturbing the sensitive parameters identified in the sensitivity analysis. We emphasize that this is a proof-of-concept study, without advising in favour of technology adoption.

2. Dynamic Modelling

The dynamic models considered describing CHO cell fermentation process performance are described. One biological cell can be recognized as a reactor, which itself grows and increases in number. The input to the “reactor” is substrate, oxygen and nutrients, which will be transformed to cells or desired products. Waste products, such as CO_2 or ammonia, are also generated. The scheme of the batch and perfusion mode fermentations in the context of API and DS manufacturing are shown in Figure 1.

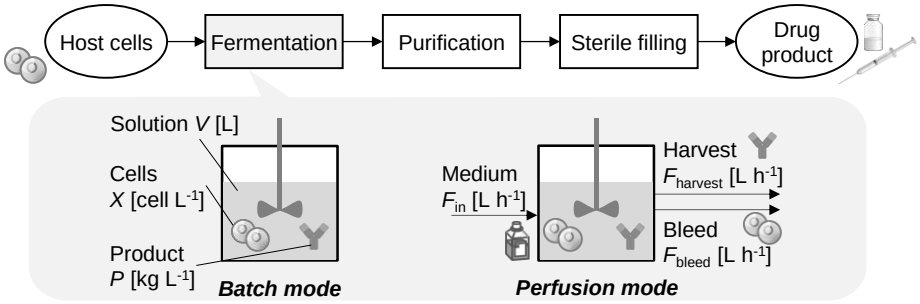

Figure 1: Typical scheme of the two culture modes of fermentation processes for biopharmaceutical manufacturing.

2.1 Model development

2.1.1 Batch mode

A CHO cell line expressing human interferon (IFN)-γ has been cultivated in 50 mL working volume at 32 and 37 °C. The culture solution was mixed at 100 rpm with a paddle agitator. The culture was initiated from highly viable and mid-exponential cells and seeded at 2.5×10^5 cells mL^{-1} with a basal medium containing 20 mM glucose (Fox et al., 2004). The mass balance equations on viable cells, glucose, and IFN-γ in the batch mode are given by Eqs. 1–3, respectively. The Monod model is assumed to be valid for predicting the specific growth rate μ and specific glucose consumption rate q_s given by Eqs. 4 and 5, respectively.

$$\frac{\mathrm{d}X_{\mathrm{batch}}}{\mathrm{d}t} = \mu_{\mathrm{batch}} X_{\mathrm{batch}} \tag{1}$$

$$\frac{\mathrm{d}S_{\mathrm{batch}}}{\mathrm{d}t} = -q_{\mathrm{S,batch}} X_{\mathrm{batch}} \tag{2}$$

$$\frac{\mathrm{d}P_{\mathrm{batch}}}{\mathrm{d}t} = q_{\mathrm{P,batch}} X_{\mathrm{batch}} \tag{3}$$

$$\mu_{\mathrm{batch}} = \frac{\mu_{\mathrm{max,batch}}\, S_{\mathrm{batch}}}{K_{\mathrm{batch}} + S_{\mathrm{batch}}} \ (S_{\mathrm{batch}} \geq S_{\mathrm{t,batch}}) = 0 \ (S_{\mathrm{batch}} < S_{\mathrm{t,batch}}) \tag{4}$$

$$q_{\mathrm{S,batch}} = \frac{q_{\mathrm{max}}\, S_{\mathrm{batch}}}{K_{\mathrm{S}} + S_{\mathrm{batch}}} \tag{5}$$

Here, t is time, and X, S and P are concentrations of viable cells, substrate, and product, respectively. The experimental values of the maximum specific growth rate μ_{max}, Monod growth constant K, maximum specific substrate consumption rate q_{max}, Monod substrate consumption constant K_s and specific production rate of product q_P at both 32 and 37 °C cultures of the CHO cell line are defined in the literature (Fox et al., 2004), with values summarized in Table 1. An assumption of the onset of massive cell death with the depletion of glucose is applied as shown in Eq. 4. The parameter S_t is the minimum substrate concentration at which cell growth was observed, i.e., substrate threshold concentration. The initial conditions are given by the experiment ($X_{0,\mathrm{batch}} = 2.5\times10^5$ cells mL^{-1} and $S_{0,\mathrm{batch}} = 3.6$ mg mL^{-1}) and by an assumption ($P_{0,\mathrm{batch}} = 0$ µg mL^{-1}).

Table 1: Parameter values used in batch (Fox et al., 2004) and perfusion mode (Karst et al., 2017a) simulations.

Parameter	**Unit**	**Batch mode**	**Perfusion mode**	**Temperature** (°C)
F_{harvest}	L hr^{-1}	–	0.083	–
K_{batch}	mg mL^{-1}	0.10	–	32
		0.80	–	37
K_S [*1]	mg mL^{-1}	1.2	–	32
		11	–	37

$K_{\mu,amm}$	mg mL^{-1}	–	0.032	–
$q_{amm,perfusion}$	mg cell^{-1} hr^{-1}	–	6.6×10^{-11}	–
q_{max}	mg cell^{-1} hr^{-1}	4.6×10^{-8}	–	32
		2.4×10^{-7}	–	37
$q_{P,batch}$ *2	µg cell^{-1} hr^{-1}	3.0×10^{-8}	–	32
		1.5×10^{-8}	–	37
$q_{P,perfusion}$ *3	µg cell^{-1} hr^{-1}	–	3.3×10^{-7}	–
$S_{t,batch}$	mg mL^{-1}	$0.01S_{0,batch}$	–	–
$\mu_{max,batch}$	hr^{-1}	0.011	–	32
		0.036	–	37
$\mu_{max,perfusion}$	hr^{-1}	–	0.038	–

*1 S was glucose in the batch mode. *2 P was IFN-γ in the batch mode. *3 P was mAb in the perfusion mode.

2.1.2 Perfusion mode

A CHO cell line expressing fully humanized mAb was cultured in 1.5 L working volume with a perfusion seed bioreactor at 36.5 °C for 26 days (Karst et al., 2017a). The culture solution was mixed at 400 rpm with a Rushton turbine impeller. The culture was initiated with cells seeded at 40×10^6 cells mL^{-1}. The cell concentration was controlled by automated manipulation of the bleed rate F_{bleed} at an average value of 0.021 L hr^{-1}. The harvest rate F_{bleed} was fixed at a constant volume exchange rate at 0.083 L hr^{-1}. The value obtained from Eq. 6 is used for F_{bleed}, and a constant value (0.083 L hr^{-1}) is used for $F_{harvest}$ in the simulation. The fresh media feed was adjusted according to gravimetric feedback to keep the reactor weight constant (Eq. 7).

$$F_{bleed} = \mu_{perfusion} V_{perfusion} \tag{6}$$

$$\frac{dV_{perfusion}}{dt} = F_{in,perfusion} - F_{out} = F_{in,perfusion} - (F_{bleed} + F_{harvest}) = 0 \tag{7}$$

The mass balance equations on viable cells, ammonia, and the mAb in perfusion culture are given by Eqs. 8–10, respectively. The concentration of ammonia *AMM*, a waste product of the fermentation process, is used for predicting the specific growth rate given by Eq. (11).

$$\frac{d(V_{perfusion} X_{perfusion})}{dt} = \mu_{perfusion} V_{perfusion} X_{perfusion} - F_{bleed} X_{perfusion} \tag{8}$$

$$\frac{d(V_{perfusion} AMM)}{dt} = q_{amm,perfusion} V_{perfusion} X_{perfusion} - F_{out} AMM \tag{9}$$

$$\frac{d(V_{perfusion} P_{perfusion})}{dt} = q_{P,perfusion} V_{perfusion} X_{perfusion} - F_{harvest} P_{perfusion} \tag{10}$$

$$\mu_{perfusion} = \frac{\mu_{max,perfusion} K_{\mu,amm}}{K_{\mu,amm} + AMM} \tag{11}$$

The experimental values of μ_{max}, ammonia growth inhibition constant $K_{\mu,AMM}$, specific ammonia production rate q_{AMM}, and q_P of the CHO cell line are defined in the literature (Karst et al., 2017a) with values summarized in Table 1. The initial conditions are as per the experiment ($X_{0,perfusion}$= 40×10^6 cells mL^{-1} and $V_{0,perfusion}$ = 1.5 L) and the assumption that there is product or ammonia present at t = 0 ($AMM_{0,perfusion}$ = 0 mg mL^{-1} and $P_{0,perfusion}$ = 0 µg mL^{-1}).

2.2 Dynamic simulation trajectories

The simulations of the equations have been conducted in MATLAB R2018a and 2018b, and the employed computers are the ThinkPad-Windows 10 Pro (Intel® Core™ i5-8350U CPU @ 1.70GHz with installed memory (RAM) of 16.0GB) and ThinkCentre-Windows 8.1 Pro (Intel® Core™ i7-4790 CPU @ 3.60GHz with installed memory (RAM) of 16.0GB) (same for Section 3.2 and 4.2).

2.2.1 Batch mode

Figure 2a shows the simulation results of the growth rate with MATLAB compared to the experimental results in the literature (Fox et al., 2004). For both temperatures considered, the rate increases and eventually plateaus at some glucose concentration. The rate is higher at the higher operating temperature of 37 °C. The experimental data at 32 °C does not follow the Monod model in the same way as at 37 °C due to cell characteristics that arrest growth at lower temperatures. Similarly, Figure 2b shows the simulation results of the glucose consumption rate with MATLAB compared to the experimental results in the literature (Fox et al., 2004). Again, for both temperatures there is an increase in rate followed by a plateau with increasing glucose concentration for 32 °C. However, the rate continually increases over the glucose concentration range shown.

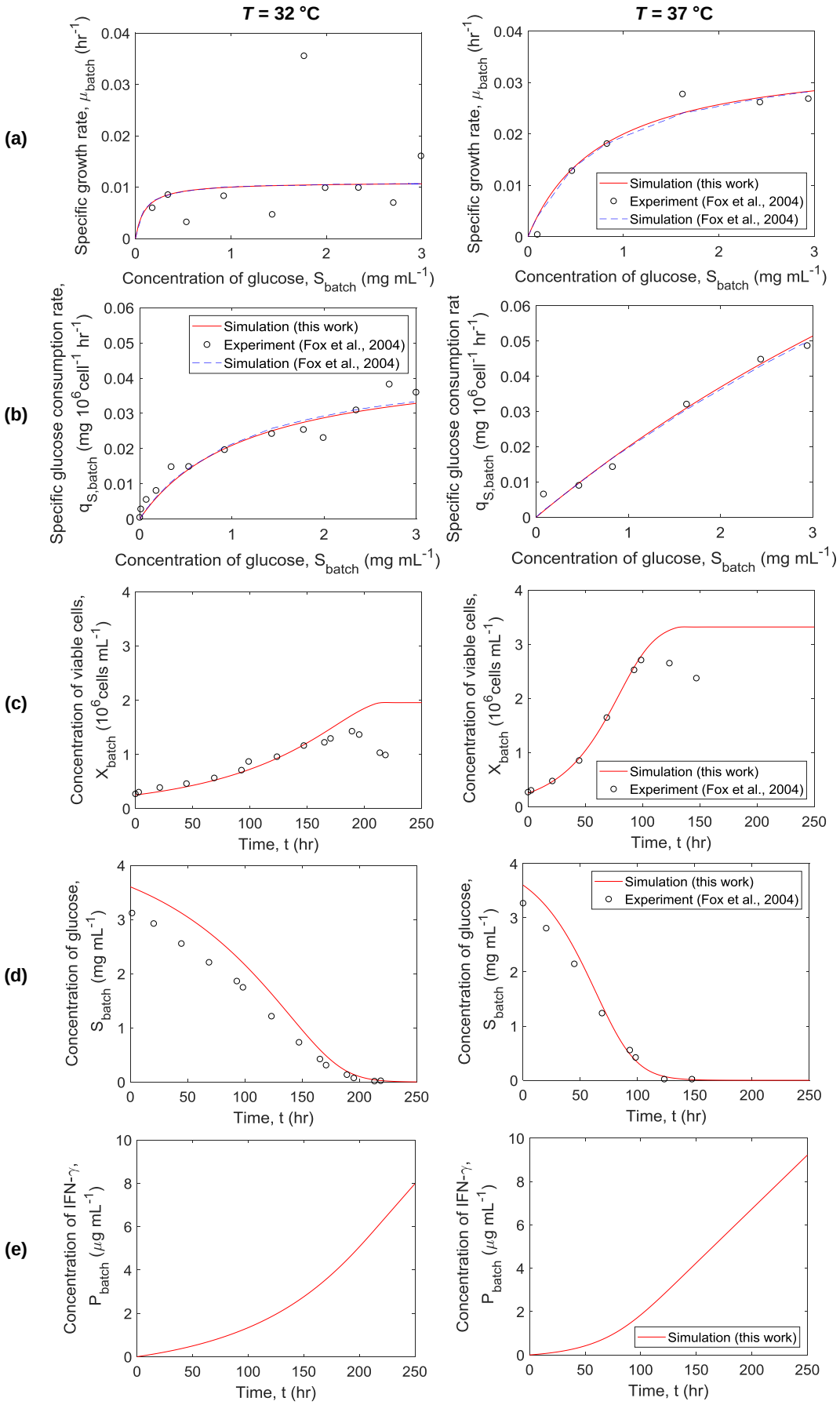

Figure 2: Batch model (Fox et al., 2004) validation vs. experimental data for (a) specific growth rates, (b) specific glucose consumption rates and concentrations of (c) viable cells, (d) glucose and (e) IFN-γ

Figure 2c-e shows the simulation results of the cell, glucose and product (IFN- γ) concentration profiles, respectively, with MATLAB compared to the experimental results in the literature (Fox et al., 2004). The simulated results reproduce the experimental results well. After approximately t = 200 hr at T = 32 °C and t = 100 hr at T = 37 °C, the experimental results show decreasing cell concentration, where the simulation results remain constant. This is because the onset of massive cell death has been considered as μ = 0 if the concentration of glucose is less than 1% of the initial concentration S_0 in the simulation with MATLAB. More accurate description of cell death kinetics incorporated into the model may reduce the discrepancy between the model and the experimental data and should be investigated. Figure 2d shows the simulated results of the glucose concentration profiles versus the experimental results (Fox et al., 2004); the simulated results show similar behaviour to the experimental results, where the concentration decreases as time passes. Figure 2e shows the simulation results of the IFN-γ concentration profiles only as there is no experimental results available in the paper. The concentration of IFN-γ increases with time. The IFN-γ concentration of the higher temperature (T = 37 °C) is smaller than that of the lower temperature (T = 32 °C) before t = 64 hr, after which the concentrations at 37 °C are higher than for 32 °C. As the batch duration proceeds, growing cells produce product and thus the batch with the higher cell concentration (i.e., that operating at higher temperature) produces more product. The advantage of mild hypothermic culture conditions on product titre are associated with prolonged culture time, (i.e., higher integral of viable cells) combined with the associated increase in specific productivity (Yoon et al., 2003; Kumar et al., 2007; Vergara et al., 2014). These positive effects may not be observed in cultures where nutrient availability limits culture duration or large numbers of cells have died.

2.2.2 Perfusion mode

Figure 3 shows the experimental results and the estimated constant values in the literature (Karst et al., 2017a), and the simulation results of different perfusion process flow rates. The estimated values in the paper were the average of fluctuating both bleed and harvest rate values over time. Constant values were also estimated regarding the values of $q_{\mathrm{AMM,perfusion}}$ and $q_{\mathrm{P,perfusion}}$, whereas the simulation results with the values did not reproduce the experimental results well. Therefore, the experimental values have been fitted using "polyval" in MATLAB. The approximate equations for $q_{\mathrm{AMM,perfusion}}$ and $q_{\mathrm{P,perfusion}}$ given by Eqs. 12 and 13, respectively. The orders of the polynomials in Eqs. 12 and 13 were chosen to that fit the experimental data well rather than based on any physical theories or process models.

$$q_{\mathrm{AMM,perfusion}} = -1.56\times10^{-20}\,t^4 + 1.90\times10^{-17}\,t^3 - 7.69\times10^{-15}\,t^2 + 1.24\times10^{-12}\,t + 1.89\times10^{-11} \quad (12)$$

$$q_{\mathrm{P,perfusion}} = 1.67\times10^{-12}\,t^2 - 1.63\times10^{-9}\,t + 6.29\times10^{-7} \quad (13)$$

Figure 4a shows the experimental results of the growth rate from the literature (Karst et al., 2017a) and MATLAB simulation results to derive the growth rate. Figure 4a-c show the results of the experimental data and fitting curve of ammonia production rate and mAb production rate, where both curves fit the experimental results well. The specific growth rate overestimates in the beginning, where the simulation mostly reproduces the experimental results well.

Published models for both batch (Fox et al., 2004) and perfusion (Karst et al., 2017a) modes were used for simulation of different fermentation processes. The model does not capture oscillations in bleed and harvest rates (Figs. 2 and 3); a constant value of harvest rate (F_{harvest} = 0.083 L hr^{-1}), taken as the average value from the literature (shown in Fig. 3), is implemented. Mechanistic model-based descriptions of these processes may provide deeper insight into optimal operating modes for different CHO culture processes.

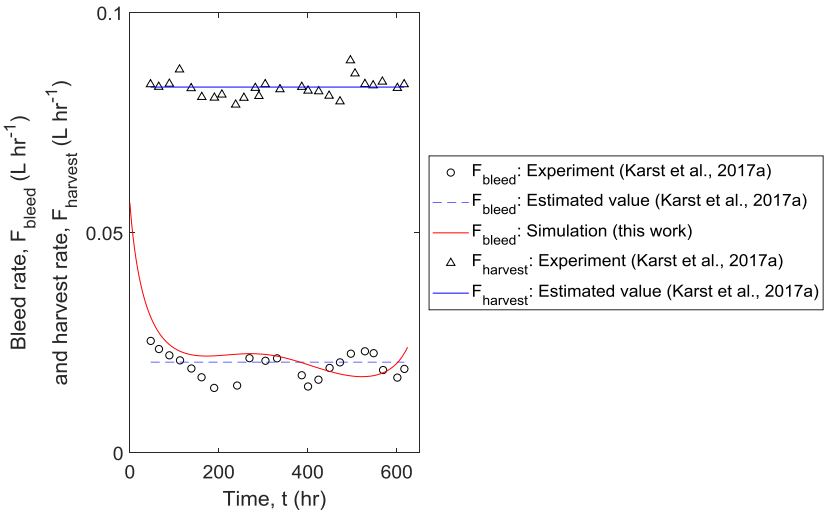

Figure 3: Profile of the flow rates for perfusion mode.

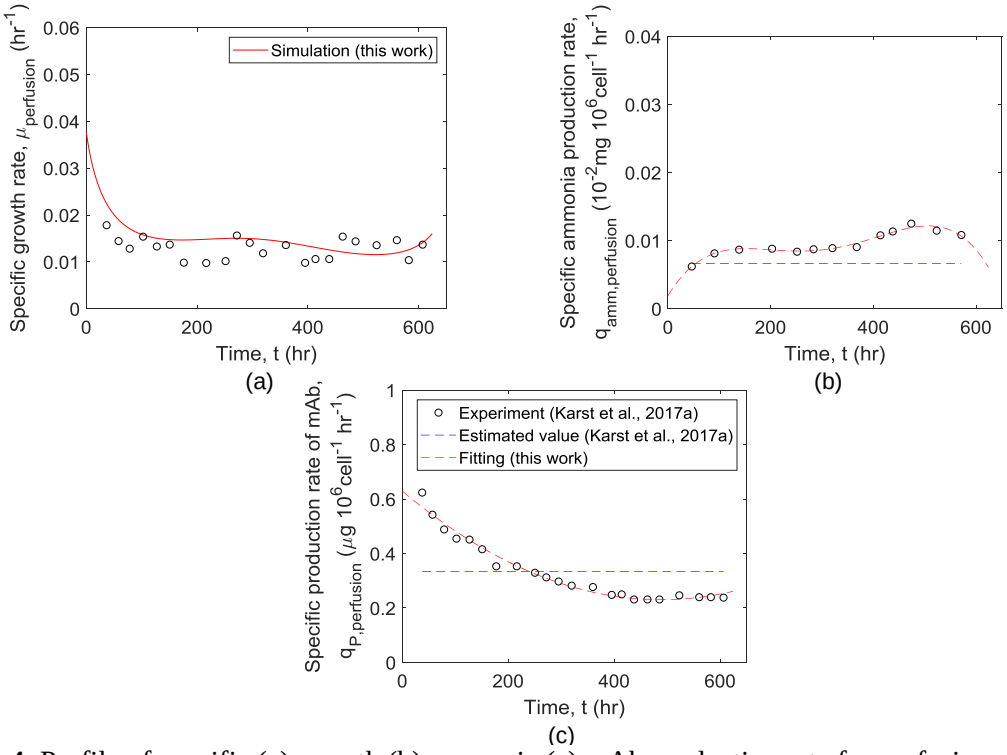

Figure 4: Profile of specific (a) growth (b) ammonia (c) mAb production rate for perfusion mode.

Figure 5 shows the simulation results of cell, ammonia, and mAb concentration profiles simulated with MATLAB, and the experimental results in the paper (Karst et al., 2017a). The concentration of the viable cells are constant with time. The simulation results of the concentration of ammonia reproduce the experimental data well, while the concentration of the product, mAb, overestimated by at least 11%.

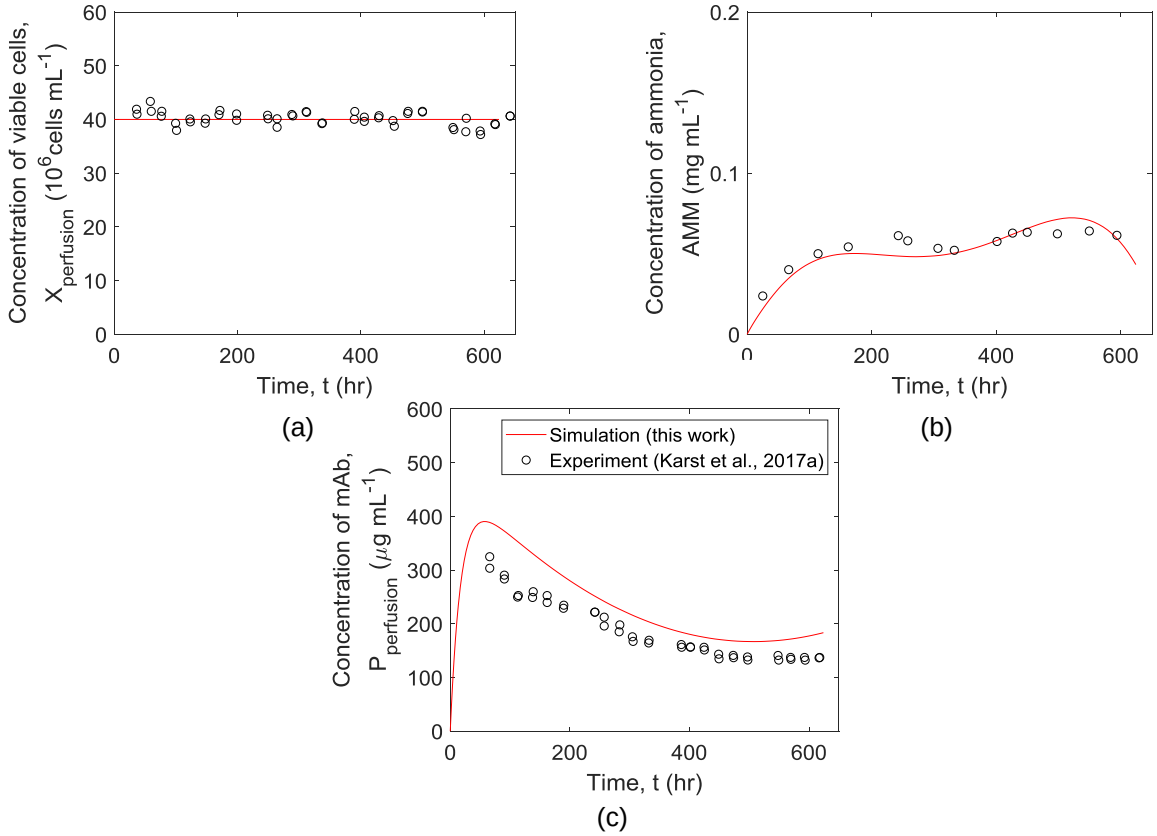

Figure 5: Profile of concentration of (a) viable cells (b) ammonia (c) mAb for perfusion mode.

2.3 Model validation

The obtained MATLAB simulation results are validated with the experimental data. The summary of the papers used for the validation of the models, and results of the validation are shown in Table 2 for batch (32 and 37 °C), and perfusion mode. The one-sample *t*-test is conducted with the null hypothesis H_0 and the alternative hypothesis H_1 are given by Eqs. 14 and 15, respectively,

$$H_0: ave_i = 0 \tag{14}$$

$$H_1: ave_i \neq 0 \tag{15}$$

$$ave_i = \frac{1}{n}\sum_{j=1}^{n}\left(i_j - \hat{i}_j\right) \tag{16}$$

where *ave* is the mean of the difference between the MATLAB simulation reuslts i_j and the experimental values $\hat{i}_j$ for each dynamic state *i* (mean bias error, MBE) with a number of data point *n* given by Eq. 16. The obtained *p*-value is shown in Table 2: the agreement level is judged as "Poor" when the value is smaller than the significant level (5%) and "Good" when the value is ≥ 50%. Standard error (SE) values are included in Table 2 for comparison between models and experimental results. More elaborate methods for validity testing exist, such as χ^2 analysis, may be employed by an interested reader, provided the experimental and model results presented in the literature (Fox et al., 2004; Karst et al., 2017a) and this work.

3. Sensitivity Analysis

3.1 Method

Sensitivity analysis is conducted for dynamic states *i* of the two culture modes. This paper has implemented a local sensitivity analysis, i.e. the One-At-a-Time (OAT) method, in order to investigate and comparatively evaluate each of the isolated (elementary) effects on each dynamic biochemical state variable as a result of perturbing each of several various model and design

parameters on for each considered fermentation mode. Local sensitivity analysis methods are suitable for models with relatively small DAE systems (Saltelli et al., 2005), as is the case for both fermentation modes and models considered in this study (Fox et al., 2004; Karst et al., 2017). More elaborate methods for quantifying and understanding parametric uncertainty are also available and widely employed in the literature, e.g. Morris Screening (Morris, 1991; Quiepo et al., 2005) and Global Sensitivity Analysis (Sobol, 2001; Li et al., 2010; Kiparissides et al., 2015); nevertheless, their implementation escapes the purpose and priorities of this study, which is the quantitative characterisation, visualisation and hopeful guiding of further experimentation on these parametric effects, for the purpose of dynamic simulation and consequent economic evaluation of different CHO fermentation modes. The analysed dynamic states are X, S and P for batch mode. The concentration of ammonia AMM is analysed in perfusion mode instead of S. In perfusion mode, the analysis of V as a dynamic state has also been conducted. Parameters in the equations to derive the dynamic states are perturbed one by one with three different perturbation ranges, $\theta = \{\pm 10, \pm 20, \pm 50\%\}$, and the effect ratio R is given by Eq. 17,

$$R = \frac{i_{0,\text{perturbed}} - i_{\text{end,perturbed}}}{i_{0,\text{basecase}} - i_{\text{end,basecase}}} - 1 \tag{17}$$

where $i_{0,\text{basecase}}$ is initial concentration of a dynamic state with no perturbations, $i_{0,\text{perturbed}}$ is initial concentration of a dynamic state with one parameter perturbed, $i_{\text{end,basecase}}$ is the final concentration of the dynamic state with no parameters perturbed and $i_{\text{end,perturbed}}$ is the final concentration with one of the parameters perturbed.

Table 2: Agreement level with experimental data of (a) batch mode (Fox et al., 2004) and (b) perfusion mode (Karst et al., 2017a) comparing with our MATLAB simulation.

Batch mode

Parameter	**Literature**	**Model**	**Agreement**		***p*-value**		**Standard Error (SE)**	
			32 °C	37 °C	32 °C	37 °C	32 °C	37 °C
μ_{batch} (hr^{-1})	✓	✓	Good	Good	0.69	0.69	7.8×10^{-3}	1.5×10^{-3}
$q_{\text{S,batch}}$ ($\text{mg } 10^6 \text{ cell}^{-1} \text{ hr}^{-1}$)	✓	✓	Acceptable	Good	0.19	0.73	3.1×10^{-3}	1.7×10^{-3}
X_{batch} (cell mL^{-1})	✗	✓	Acceptable	Acceptable	0.085	0.15	3.6×10^{5}	2.8×10^{5}
S_{batch} (mg mL^{-1})	✗	✓	Poor	Acceptable	8.3×10^{-5}	0.080	0.21	0.15
P_{batch} ($\mu\text{g mL}^{-1}$)	✓	✓	Acceptable	Acceptable	0.10	0.24	2.3	1.1

Perfusion mode

Parameter	**Literature**	**Model**	**Agreement level**	***p*-value**	**Standard Error (SE)**
$\mu_{\text{perfusion}}$ (hr^{-1})	✗	✓	–	–	–
$q_{\text{AMM,perfusion}}$ ($\text{mg } 10^6 \text{ cell}^{-1} \text{ hr}^{-1}$)	✗	✓	–	–	–
$q_{\text{P,perfusion}}$ ($\text{mg } 10^6 \text{ cell}^{-1} \text{ hr}^{-1}$)	✗	✓	–	–	–
$X_{\text{perfusion}}$ (cell mL^{-1})	✗	✓	Good	0.56	1.3×10^{6}
AMM (mg mL^{-1})	✗	✓	Acceptable	0.12	8.2×10^{-3}
$P_{\text{perfusion}}$ ($\mu\text{g mL}^{-1}$)	✗	✓	Acceptable	0.29	81

3.1.1 Batch mode

Firstly, the sensitivity of the parameters K_{batch}, K_S, q_{max}, $q_{P,batch}$, $\mu_{max,batch}$ and $S_{t,batch}$ on dynamic states X_{batch}, S_{batch} and P_{batch} are tested. The values of the parameters in the base cases are shown in Table 1. Two sensitivity analyses are conducted using values at 32 °C and 37 °C. Secondly, the parameters for initial conditions, such as $X_{0,batch}$, $S_{0,batch}$ and $P_{0,batch}$, are perturbed to investigate their effects on their respective dynamic states. The values of the parameters in the base case are shown in Section 2.1.1. Two sensitivity analyses are conducted using values at 32 and 37 °C.

3.1.2 Perfusion mode

Firstly, the sensitivity of the parameters $F_{harvest}$, $K_{\mu,AMM}$, $q_{AMM,perfusion}$, $q_{P,perfusion}$ and $\mu_{max,perfusion}$ on dynamic states $X_{perfusion}$, AMM, $P_{perfusion}$, and $V_{perfusion}$ are tested. The values of the parameters in the base case are shown in Table 1. Secondly, the parameters for initial conditions, such as $X_{0,perfusion}$, $AMM_{0,perfusion}$, $P_{0,perfusion}$ and $V_{0,perfusion}$, are perturbed to investigate their effects on their respective dynamic states. The values of the parameters in the base cases are shown in Section 2.1.2.

3.2 Sensitivity analysis results

The effect ratio has been calculated as an indicator of the sensitivity of the parameter on dynamic states. The ratio has been derived for six different perturbation ratio and the ratio has been categorized into two patterns that are negative perturbation, -10%, -20%, and -50%, as well as a positive perturbation, 10%, 20%, and 50%.

3.2.1 Batch mode

Table 3 shows the effect ratio R for the batch mode at 32 and 37 °C, where the parameters. At 32 °C, the parameters that have the value of R more than 0.5 are q_{max} and $\mu_{max,batch}$ on X_{batch}, as well as $q_{P,batch}$ and $\mu_{max,batch}$ on P_{batch} as shown in Table 3 for the perturbation ratio of 50%. This tendency is similar at 37 °C as shown in Table 3, however, $\mu_{max,batch}$ has a smaller effect on X_{batch}, and q_{max} has a much larger effect on P_{batch}. The effect ratio of the parameters on S_{batch} is observed small in common to both temperatures except for $S_{0,batch}$.

3.2.2 Perfusion mode

Table 3 shows the effect ratio R for perfusion mode. In the perfusion mode, no effect on $X_{perfusion}$ and $V_{perfusion}$ are observed (R = 0) due to the constant concentration of the viable cells and the culture volume. The parameters that have the value of R > 0.5 are $F_{harvest}$ on AMM and $P_{perfusion}$ as shown in Table 3 for the perturbation ratio of 50%. Also, $X_{0,perfusion}$ and $V_{0,perfusion}$ have the value of R > 0.5 for both AMM and $P_{perfusion}$ for the perturbation ratio of 50%.

3.2.3 Commonality among two culture modes

Although the operating parameters are different between batch and perfusion culture modes due to the inherently different nature of their operation, there is some commonality between the two methods. The parameters for each mode's model are categorized into kinetic and operation parameters. Kinetic parameters are, e.g., K, q and μ, whereas operating parameters which can be altered in the design stages are flowrates (for perfusion mode) and initial conditions of the cultures (e.g., initial cell and/or substrate concentration). In common to all the culture modes, kinetic parameters have significant effect on dynamic states of X and P; however, for perfusion mode, X is maintained constant by appropriate selection of harvest and bleed rates to maintain steady production in an effort towards continuous operation. In particular, the parameters that directly affect specific growth, substrate consumption rates and product production are found to be sensitive. The harvest rate is observed to be sensitive in perfusion mode. The sensitivity of different initial conditions varies between the culture modes, but at least one initial concentration is found to have large sensitivity on at least one dynamic state in both cases.

The batch mode results in different sensitivity at different temperature for the parameter q_{max}. Experimental data is used to observe the difference in process performance as a function of temperature for batch mode, with Arrhenius-type equations for different parameters being unavailable for this process or for CHO cell fermentations. Availability of such temperature-dependence

modelling would also allow process performance to be assessed at intermediated temperatures to those considered here, i.e., 32 °C < T < 37 °C. Previous work in the literature investigated the effect of temperature on cellular response or productivity (Masterton and Smales, 2014).

4. Process Design

The dynamic models are applied to investigate the design space and perform economic evaluations of both batch and perfusion modes described. Quantitative measures of process performances for design include culture time, media usage, productivity and economic indicators such as total costs. In this work, culture time to produce a target amount of product and the annual operating cost are computed.

Table 3: Effect ratio on dynamic states with $|R| \geq 0.5$ in bold.

Batch mode (T = 32 °C)

Parameters	X_{batch}		S_{batch}		P_{batch}	
θ	–50%	50%	–50%	50%	–50%	50%
K_{batch}	1.27×10^{-1}	-5.72×10^{-2}	3.51×10^{-4}	-3.62×10^{-4}	6.10×10^{-2}	-3.84×10^{-2}
K_S	-2.67×10^{-1}	2.94×10^{-1}	7.53×10^{-4}	-4.28×10^{-3}	-1.09×10^{-1}	7.25×10^{-2}
q_{max}	$\mathbf{7.72\times10^{-1}}$	-3.22×10^{-1}	-4.87×10^{-2}	7.17×10^{-4}	1.51×10^{-1}	-1.42×10^{-1}
$q_{P,batch}$	6.51×10^{-3}	2.59×10^{-2}	1.12×10^{-5}	4.72×10^{-5}	-4.99×10^{-1}	$\mathbf{5.09\times10^{-1}}$
$\mu_{max,batch}$	$\mathbf{-6.12\times10^{-1}}$	$\mathbf{5.23\times10^{-1}}$	-1.03×10^{-1}	7.57×10^{-4}	$\mathbf{-5.13\times10^{-1}}$	$\mathbf{6.31\times10^{-1}}$
$S_{t,batch}$	3.88×10^{-2}	3.30×10^{-3}	6.15×10^{-5}	6.72×10^{-6}	8.40×10^{-3}	8.29×10^{-4}
$X_{0,batch}$	-1.14×10^{-1}	1.21×10^{-2}	-4.87×10^{-2}	7.16×10^{-4}	-4.24×10^{-1}	2.85×10^{-1}
$S_{0,batch}$	-3.11×10^{-1}	3.15×10^{-1}	$\mathbf{-5.00\times10^{-1}}$	4.99×10^{-1}	-1.65×10^{-1}	1.06×10^{-1}
$P_{0,batch}$	0	0	0	0	0	0

Batch mode (T = 37 °C)

Parameters	X_{batch}		S_{batch}		P_{batch}	
θ	–50%	50%	–50%	50%	–50%	50%
K_{batch}	3.22×10^{-1}	-1.78×10^{-1}	1.99×10^{-6}	-1.76×10^{-5}	2.99×10^{-1}	-1.69×10^{-1}
K_S	-4.45×10^{-1}	4.53×10^{-1}	1.98×10^{-6}	-6.75×10^{-6}	-3.53×10^{-1}	3.24×10^{-1}
q_{max}	$\mathbf{9.96\times10^{-1}}$	-3.30×10^{-1}	-1.40×10^{-5}	1.57×10^{-6}	$\mathbf{6.93\times10^{-1}}$	-2.60×10^{-1}
$q_{P,batch}$	5.28×10^{-3}	1.30×10^{-3}	9.25×10^{-8}	2.11×10^{-8}	-4.98×10^{-1}	$\mathbf{5.01\times10^{-1}}$
$\mu_{max,batch}$	-4.95×10^{-1}	$\mathbf{5.03\times10^{-1}}$	-2.51×10^{-3}	2.04×10^{-6}	$\mathbf{-5.30\times10^{-1}}$	$\mathbf{5.67\times10^{-1}}$
$S_{t,batch}$	1.32×10^{-2}	-6.08×10^{-3}	1.94×10^{-7}	-1.12×10^{-7}	7.47×10^{-3}	-3.52×10^{-3}
$X_{0,batch}$	5.28×10^{-3}	3.29×10^{-3}	-1.33×10^{-5}	1.57×10^{-6}	-1.50×10^{-1}	1.09×10^{-1}
$S_{0,batch}$	-3.40×10^{-1}	2.61×10–1	$\mathbf{-5.00\times10^{-1}}$	$\mathbf{5.00\times10^{-1}}$	-3.16×10^{-1}	2.32×10^{-1}
$P_{0,batch}$	0	0	0	0	0	0

Perfusion mode

Parameters	$X_{perfusion}$		AMM		$P_{perfusion}$		$V_{perfusion}$	
θ	–50%	50%	–50%	50%	–50%	50%	–50%	50%
$F_{harvest}$	0	0	**1.19**	-3.51×10^{-1}	$\mathbf{9.61\times10^{-1}}$	-3.28×10^{-1}	0	0
$K_{\mu,AMM}$	0	0	1.15×10^{-1}	-6.94×10^{-2}	-2.10×10^{-6}	5.11×10^{-6}	0	0
$q_{AMM,perfusion}$	0	0	0	0	0	0	0	0
$q_{P,perfusion}$	0	0	0	0	0	0	0	0
$\mu_{max,perfusion}$	0	0	1.49×10^{-1}	-1.33×10^{-1}	-1.82×10^{-6}	-9.21×10^{-6}	0	0
$X_{0,perfusion}$	0	0	$\mathbf{-5.56\times10^{-1}}$	$\mathbf{6.04\times10^{-1}}$	$\mathbf{-5.00\times10^{-1}}$	$\mathbf{5.00\times10^{-1}}$	0	0
$AMM_{0,perfusion}$	0	0	0	0	0	0	0	0
$P_{0,perfusion}$	0	0	0	0	0	0	0	0
$V_{0,perfusion}$	0	0	$\mathbf{-5.17\times10^{-1}}$	$\mathbf{5.73\times10^{-1}}$	$\mathbf{-4.94\times10^{-1}}$	$\mathbf{4.84\times10^{-1}}$	0	0

4.1 Method

The target amount of product is determined based on the information of the required amount to produce one vial of product. Information of some drug products that use IFN-γ (for batch mode) or mAb (perfusion mode) is reviewed. It is assumed that the production amount per year is 20,000 vials per year for both products. The desired amount w is determined as shown in Table 4. Inefficiencies associated with downstream processing following the fermentation process are not considered. Annual operating cost for the required time to produce the certain amount of products involves raw material cost, utility cost, and waste treatment cost. Costing data used in this work is summarized in Table 4.

The chosen scale of operation for both culture volumes (100 L) for economic evaluations correspond to experimental demonstration values (Fox et al, 2004; Karst et al., 2017a). Conclusions drawn about economic evaluations from these results correspond to the implemented production scale. Larger production scales closer to industrial application ranges can be readily considered in the implemented methodology and framework for comparison purposes.

Table 4: Target amounts of active pharmaceutical ingredients (APIs) and drug products (DPs) with costing data.

API	Desired amount, w [μg yr^{-1}]	API per vial	Unit	Source
IFN-γ	10^7	500	μg/vial	[1], [2]
mAb	2×10^9	100	mg/vial	[3], [4]

Cost Component	Description	Unit	Value	Source
C_{cell}	CHO cells	USD cell^{-1} mL	9.36×10^{-4}	[5]
C_{media}	Culture media	USD mL^{-1}	0.11	[6]
$C_{electricity}$	Electricity	USD kWh^{-1}	1.59×10^3	[7]
C_{waste}	Waste treatment	USD L^{-1}	0.46	[8]

[1] https://ds-pharma.jp/product/sumiferon/
[2] (Meager et al., 2001)
[3] http://www.info.pmda.go.jp/go/pack/4291413A1022_1_20/4291413A1022_1_20?view=body
[4] http://www.info.pmda.go.jp/go/pack/4291406D3021_1_04/
[5] http://www.saibou.jp/products/cho/cho.php
[6] https://www.gelifesciences.co.jp/catalog/39552.html
[7] Department for Business, Energy & Industrial Strategy "Industrial electricity prices in the IEA" (2018)
[8] (Schaber et al., 2011)

4.1.1 Evaluation indicators

The annual production time t' required to produce the amount w is given by Eqs. 18 and 19 for batch and perfusion modes, respectively:

$$V_{\text{working}} f(t') = w \tag{18}$$

$$F_{\text{harvest}} \int_0^{t'} P' \, \mathrm{dt} = w \tag{19}$$

where V_{working} is the working culture volume and P' is the product concentration at t'. The working volume is estimated as 100 L for both culture modes. The symbol f is the function to derive the concentration of product for batch and perfusion culture.

$$P' = f(t') \tag{20}$$

In this calculation, the limited production time of batch mode is defined as the time where the substrate concentration S_{batch} reached to the threshold concentration $S_{\text{t,batch}} = 0.01 S_{\text{0,batch}}$ and the time for perfusion mode is defined as the maximum time when the experiment was conducted (= 624 hr). The annual operating cost C_{total} for both culture modes is given by

$$C_{\text{total}} = C_{\text{material}} + C_{\text{utility}} + C_{\text{waste}}\ V_{\text{media}} \quad (21)$$

$$C_{\text{material}} = C_{\text{cell}}\ X_0 + C_{\text{media}}\ V_{\text{media}} \quad (22)$$

$$C_{\text{utility}} = C_{\text{electricity}}\ \left(Q_{\text{heating}} + P_{\text{mixing}}\ t'\right) \quad (23)$$

$$V_{\text{media}} = V_{\text{working}}\ \text{(batch mode)} \quad (24)$$
$$= V_{\text{working}} + F_{\text{in,perfusion}}\ t'\ \text{(perfusion)}$$

where the raw material cost C_{material} and the utilities cost C_{utility} are given by Eqs. 22 and 23, respectively. The volume of culture media V_{media} is given by Eq. 24. The energy for heating the reactor Q_{heating} and power for mixing P_{mixing} given by Eqs. 25–27, respectively,

$$Q_{\text{heating}} = m_{\text{solution}}\ c_{\text{P}}\ \Delta T \quad (25)$$

$$m_{\text{solution}} = \rho_{\text{solution}} V_{\text{media}} \quad (26)$$

$$P_{\text{mixing}} = k\,\mu_{\text{solution}}\ N^2\ D^3\ \text{(Laminar flow when } Re < 10 - 100) \quad (27)$$
$$= N_{\text{P}}\ \rho_{\text{solution}}\ N^3 D^5 \left(\text{Turbulent flow when } Re > 10^3\right)$$

$$Re = \frac{N\,D^2 \rho_{\text{solution}}}{\mu_{\text{solution}}} \quad (28)$$

where m_{solution} is the mass of solution, c_{P} is the specific heat capacity and ΔT the difference between reaction and room temperatures. Energy from endo- or exothermicity of the reaction and heat losses are neglected. The parameters μ_{solution}, ρ_{solution}, N and D are the viscosity of the solution, density of the solution, stirring speed and impeller blade diameter, respectively. The constants k and N_{P} have different values depending on the type of the blade. The Reynolds number Re is given by Eq. 28. Electricity costs assume a 40% efficiency.

Given a certain interest rate r and production lifetime LT, the net present cost NPC is calculated by Eq. 29:

$$NPC = \sum_{j=1}^{LT} \frac{C_{\text{total}}}{(1+r)^j} \quad (29)$$

where, the interest rate is considered 5% and the production lifetime is assumed to be 20 years.

We define NPC as an economic-based function for comparative evaluation purposes. Whilst formulating a formal optimisation problem for NPC minimisation can elucidate optimal operating strategies, our focus is to evaluate different fermentation modes in terms of different evaluation indicators: NPC and production time.

4.1.2 Design variables

Based on the sensitivity analysis in Section 3, the parameters with large sensitivity on the product concentration have been selected for tuning in process design for each culture modes. For the batch mode, the initial cell and substrate (glucose) concentrations, X_0 and S_0, are varied for process design while for perfusion mode, initial cell concentration, X_0 and harvest rate, F_{harvest}, are varied.

4.2 Results and discussion

4.2.1 Batch mode

The annual batch number to produce the desired amount is shown in Fig. 6a for varying initial concentration of viable cells and initial glucose concentration. The case of the viable cells had the same batch number for each production temperature. On the other hand, the batch number differed

depending on the value of the initial concentration of glucose, which directly affected the limited production time.

The annual production time per year is shown in Fig. 6b for the case perturbing the initial concentration of viable cells and for varying initial glucose concentration. In both initial cell and glucose concentration variations, the production time decreases due to the increasing produced amount of IFN-γ per batch. The difference of the production amount led to the smaller annual batch numbers in larger concentrations, which results in the shorter production time per year. The higher temperature (T = 37 °C) always results in longer production times than lower temperature (T = 32 °C).

The net present cost (*NPC*) is shown in Fig. 6c. The case of perturbing the initial concentration of glucose results in the same tendency for both temperatures, where the *NPC* decreased as the concentration becomes larger. The value is similar among the initial glucose concentrations resulting in the same annual batch per year.

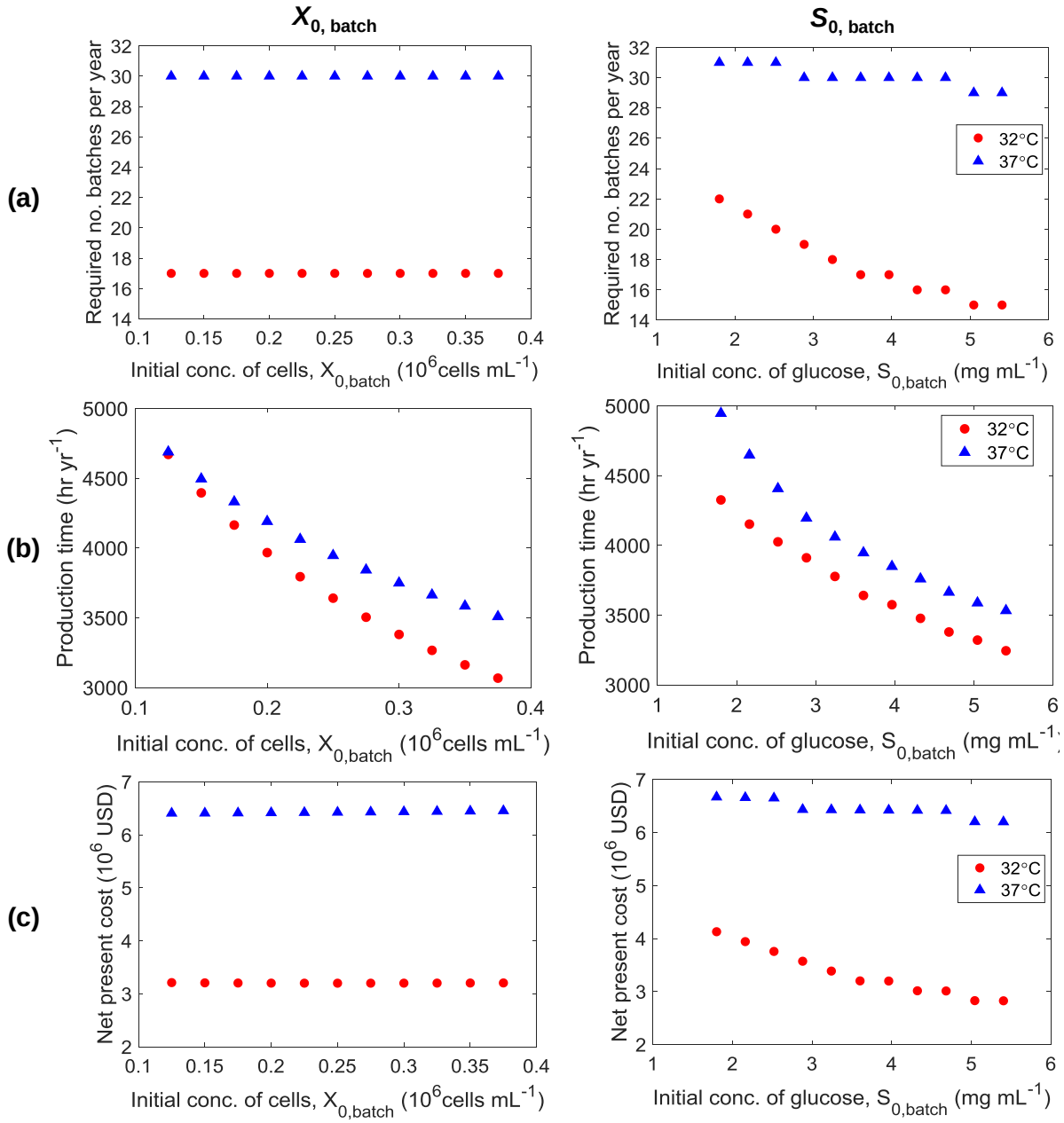

Figure 6: Effect of perturbations in initial cell (X_0) and glucose (S_0) concentrations on (a) annual number of batches, (b) annual total production time and (c) net present costs for batch mode.

The breakdown of the *NPC* for batch mode is shown in Fig. 8. In common to all the cases, the effect of cell purchase and waste treatment are small. The waste cost is not shown as it is insignificant in comparison to the other cost components shown. The cell purchase cost increases as the initial cell concentration increases and the waste treatment cost decreases with decreasing production time and increasing concentrations. The mixing cost also becomes smaller as the production time decreases. Media costs are the most significant contributor, which decreases with increasing cell concentration.

4.2.2 Perfusion mode

The annual production time per year for perfusion mode is shown in Fig. 7a. The production time decreases as the values of the harvest rate, and the initial cell concentration increased. For the case of the harvest rate, the outlet flow increased as the harvest rate increases, which leads to ammonia (waste product) to be removed faster so that the product concentration increased - higher product concentration results in shorter production time. As the initial cell concentration increases, productivity increases also. The effect of varying initial cell concentration on annual production time is more significant than for varying harvest rate.

The *NPC* is shown in Fig. 7b for the case perturbing harvest rate and for the case perturbing the initial concentration of viable cells. The decrease of the *NPC* corresponds to the decreased production time. The change of the *NPC* is larger in the case of perturbing the initial cell concentration than the case of perturbing the harvest rate, as is the case in the annual production time.

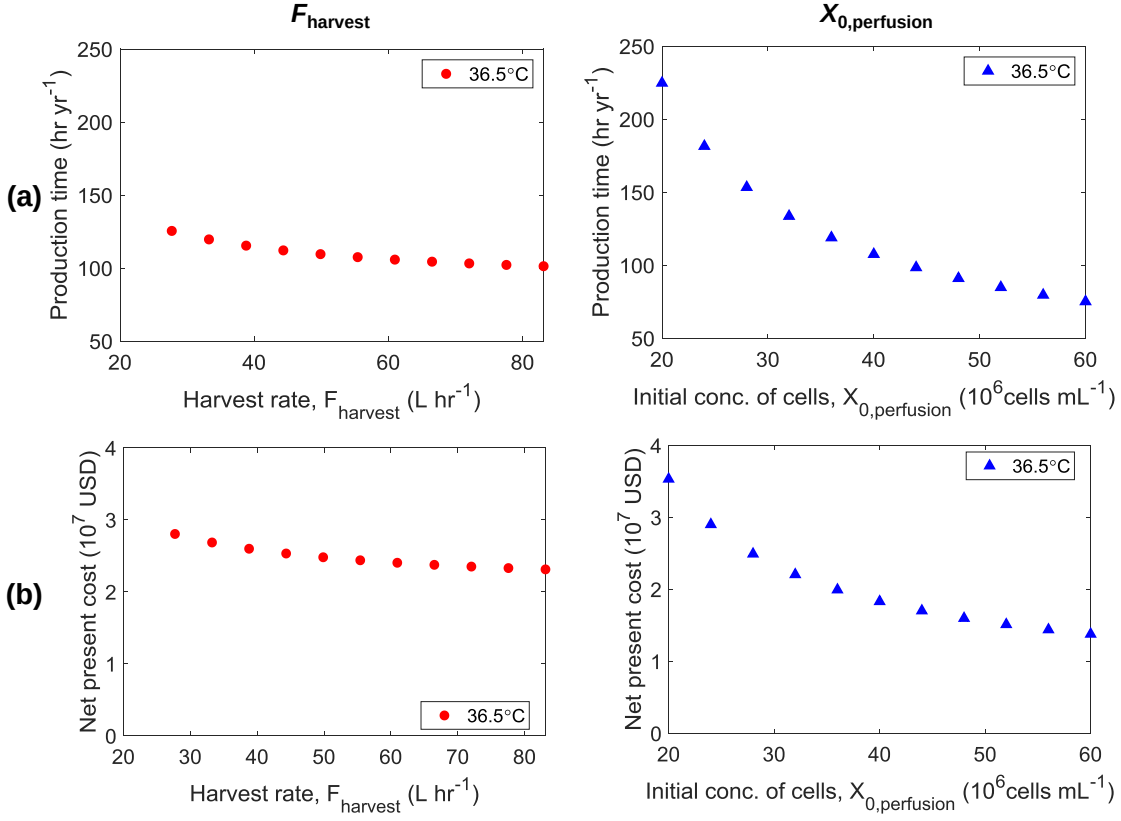

Figure 7: Effect of perturbations in harvest rate ($F_{harvest}$) and initial cell concentration (X_0) on (a) annual number of batches, (b) annual total production time and (c) net present costs for perfusion mode.

The breakdown of the *NPC* results is shown in Fig. 8 for the case perturbing the harvest rate and for the case perturbing the initial concentration of viable cells. In common to all the cases, the effect of cell purchase and waste treatment are small. Similarly to the batch mode results, waste cost components are not shown as their contribution is insignificant in comparison to other cost

components, although it has been explicitly considered. The cell purchase cost increases as the initial cell concentration increases. Cost related to media is known to be dominant especially in the case of perfusion mode (Klutz et al., 2016). The mixing cost becomes smaller as the production time becomes shorter.

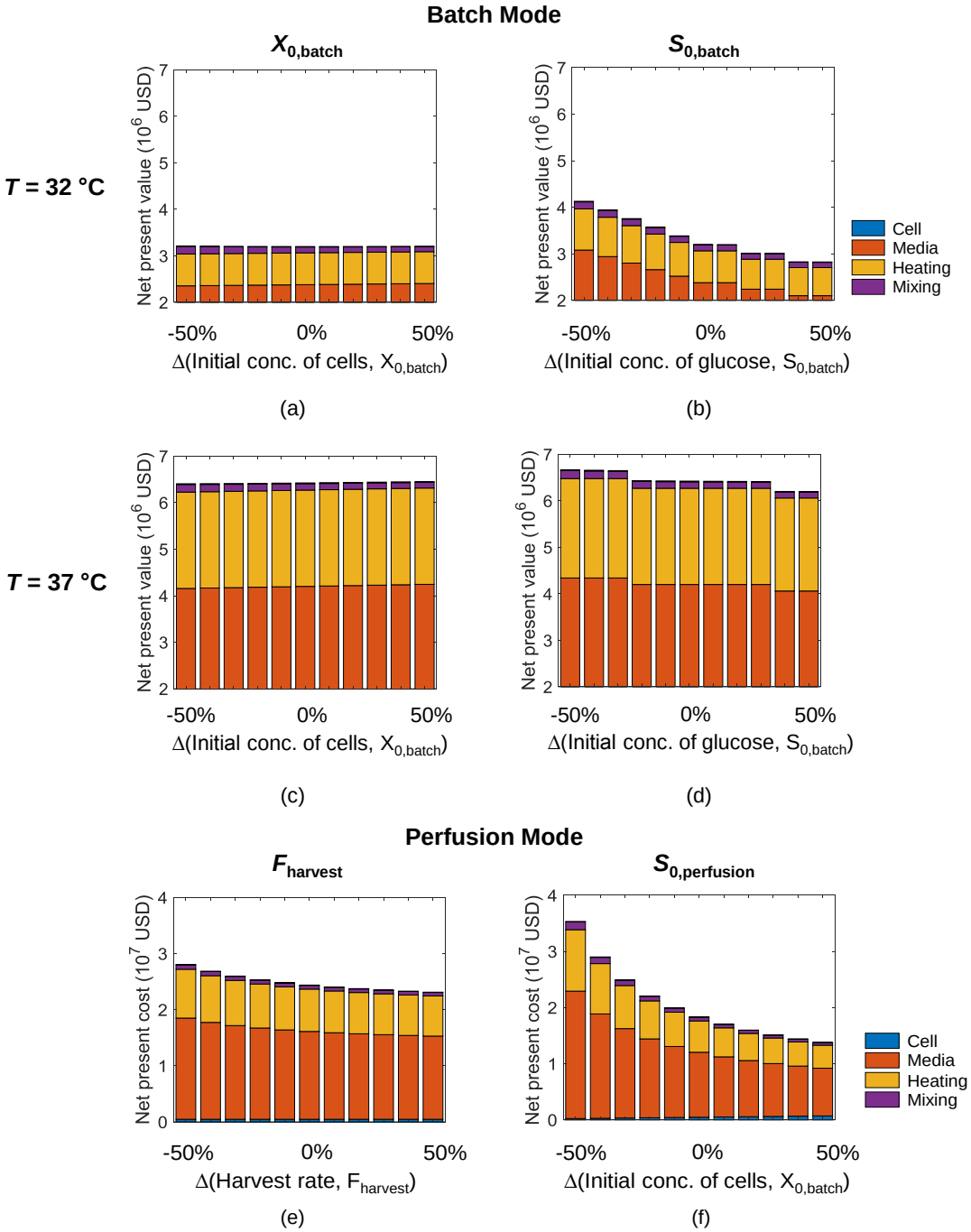

Figure 8: Batch Mode: Detailed breakdown of net present cost with perturbation of (a) initial cell concentration and (b) initial glucose concentration at T=32 °C, (c) initial cell concentration and (d) initial glucose concentration at T=37 °C. Perfusion Mode: Detailed breakdown of net present cost with perturbation of (e) harvest rate and (f) initial cell concentration.

5. Conclusions

The dynamic models of the two modes of the CHO cell-based production have been developed and simulated with MATLAB. These two modes are namely a batch mode (the conventional mode in biopharmaceutical manufacturing processes), and a perfusion mode (recently introduced towards continuous manufacturing). In this work, a batch mode to produce interferon and a perfusion mode to produce monoclonal antibody have been analysed. The simulation results have been compared to experimental data available from the literature (Fox et al., 2004; Karst et al., 2017a). For both culture modes, the one-sample *t*-test has been conducted as a sensitivity analysis for every dynamic state of the models, and the *p*-value has been used as a quantitative indicator to probe agreement between simulation and experimental data.

A sensitivity analysis has also been conducted by applying the developed models of the batch and perfusion mode. Nine parameters for batch and perfusion are perturbed with ±10, ±20 and ±50 % from the values of base case to see the effect on three dynamic states. In the batch mode, kinetic parameters to derive specific growth rate and specific substrate consumption rates are identified to be sensitive. In the perfusion mode, harvest rate is found to be sensitive in common to both on ammonia and product concentrations. In common to the two culture modes, initial concentration is found to be sensitive to the dynamic states. Based on the results of the sensitivity analysis, some parameters have been chosen for the analysis of process design.

In the process design, two objective functions have been defined that are the required time to produce a certain amount of product per year, and the net present cost as an economic evaluation indicator. For the batch mode and the perfusion mode, operation parameters, such as initial concentration of viable cells (for the both modes), initial concentration of glucose, (only for the batch mode) and harvest rate (only for the perfusion mode), are tested by perturbing the value within the ranges of ±50%. The annual production time decreases as all the operating parameters increase. In the net present cost results, the media cost dominates for all the cases as known in biologics manufacturing. The heating cost is also relevant to the large media cost, where the usage of the media is large especially in the perfusion modes, where the media flows as an inlet. In this work, change-over costs, e.g., cleaning, are not included in the batch mode, where the multiple batches are assumed to be produced without any change-over operations. In biopharmaceutical manufacturing processes, the change-over costs are known to consume a large amount of energy cleaning and sterilization, which would exacerbate the results of the economic evaluation of the batch mode.

In the future, the incorporation of the effect of cell death behaviour is necessary to make the process design with the time indicator and the economic indicator more rigorous. The analysis of process design will also be expanded by defining other objective functions and by analysis the different design variables. Furthermore, the models will be implemented to a dynamic optimisation problem formulation to find optimal operating and design parameters.

Acknowledgements

Ms. Haruku Shirahata acknowleges the financial support of the Leading Graduates Schools Program, “Global Leader Program for Social Design and Management” by the Ministry of Education, Culture, Sports, Science and Technology as well as Grant-in-Aid for JSPS Research Fellow No. 18J13892. Mr. Samir Diab gratefully acknowledges the financial support of the Engineering and Physical Sciences Research Council (EPSRC) via a Doctoral Training Partnership (DTP) PhD Fellowship (Grant # EP/N509644/1). Dr. Hirokazu Sugiyama gratefully acknowledges Grant-in-Aid for Young Scientists (A) No. 17H04964 from the Japan Society for the Promotion of Science. Dr. Dimitrios I. Gerogiorgis gratefully acknowledges a Royal Academy of Engineering (RAEng) Industrial Fellowship. All authors also gratefully acknowledge the support of the Great Britain Sasakawa and Nagai Foundations, and declare no competing financial interest. Tabulated and cited literature data suffice for reproduction of all original results and no other supporting data are required to ensure reproducibility.

Nomenclature and Acronyms

Latin Letters and Acronyms

AMM	Concentration of ammonia, mg mL^{-1}
$AMM_{0,perfusion}$	Initial concentration of ammonia, mg mL^{-1}
ave	Mean of the difference between the MATLAB simulation results and the experimental values
ATFF	Alternating tangential flow filtration
CHO	Chinese hamster ovary
C_{cell}	Price of CHO cells, USD $cell^{-1}$ mL
$C_{electricitv}$	Price of electricity, USD kWh^{-1}
$C_{material}$	Raw material cost, USD
C_{media}	Price of culture media, USD mL^{-1}
c_P	Specific heat of the solution, J g^{-1} K^{-1}
C_{total}	Annual operating cost, USD yr^{-1}
$C_{utilitv}$	Utility cost, USD
C_{waste}	Price of waste treatment, USD L^{-1}
D	Blade diameter, m
DP	Drug product
F_{bleed}	Bleed rate, L hr^{-1}
$F_{harvest}$	Harvest rate, L hr^{-1}
$F_{in,perfusion}$	Feed rate for perfusion culture, L hr^{-1}
F_{out}	Outlet flow rate, L hr^{-1}
i	Dynamic states (MATLAB simulation), cell mL^{-1}, mg mL^{-1}, µg mL^{-1}, or L
$\hat{t}$	Dynamic states (experimental results), cell mL^{-1}, mg mL^{-1}, µg mL^{-1}, or L
$i_{0,basecase}$	Initial concentration of a dynamic state i with no parameters perturbed, cell mL^{-1}, mg mL^{-1}, µg mL^{-1}, or L
$i_{0,perturbed}$	Initial concentration of a dynamic state i with one of the parameters perturbed, cell mL^{-1}, mg mL^{-1}, µg mL^{-1}, or L
$i_{end,basecase}$	Final concentration of a dynamic state i with no parameters perturbed, cell mL^{-1}, mg mL^{-1}, µg mL^{-1}, or L
$i_{end,perturbed}$	Final concentration of a dynamic state i with one of the parameters perturbed, cell mL^{-1}, mg mL^{-1}, µg mL^{-1}, or L
IFN	Interferon
k	Constant, –
K_{batch}	Monod growth constant for batch culture, mg mL^{-1}
K_S	Monod substrate consumption constant, mg mL^{-1}
$K_{\mu,AMM}$	Ammonia growth inhibition constant, mg mL^{-1}
LT	Production lifetime, yr
$m_{solution}$	Weight of the heated solution, g
mAb	monoclonal antibody
n	Number of data points, –
N	Stirred speed, rps
N_P	Constant, –
NPC	Net present cost, USD
OUR	Oxygen uptake rate
p	Active pharmaceutical ingredients, –
P_{batch}	Concentration of product for batch culture, µg mL^{-1}
$P_{perfusion}$	Concentration of product for perfusion culture, µg mL^{-1}
P_{mixing}	Power for mixing of a propeller in a reactor, W
P'	Concentration of product at time t', µg mL^{-1}
$P_{0,batch}$	Initial concentration of product for batch culture, µg mL^{-1}
$P_{0,perfusion}$	Initial concentration of product for perfusion culture, µg mL^{-1}
$Q_{heating}$	Energy for heating up a reactor, J

$q_{AMM,perfusion}$	Specific ammonia production rate for perfusion culture, mg cell^{-1} hr^{-1}
q_{max}	Maximum specific substrate consumption rate, mg cell^{-1} hr^{-1}
$q_{P,batch}$	Specific production rate of product for batch culture, µg cell^{-1} hr^{-1}
$q_{P,perfusion}$	Specific production rate of product for perfusion culture, µg cell^{-1} hr^{-1}
$q_{S,batch}$	Specific substrate consumption rate for batch culture, mg cell^{-1} hr^{-1}
r	Interest rate, –
R	Effect ratio, –
Re	Reynolds number, –
S_{batch}	Concentration of substrate for batch culture, mg mL^{-1}
$S_{t,batch}$	Substrate threshold concentration for batch culture, mg mL^{-1}
$S_{0,batch}$	Initial concentration of substrate for batch culture, mg mL^{-1}
SE	Standard error
t	Time, hr
t'	Annual production time to produce the desired amount, hr yr^{-1}
T	Temperature, °C
ΔT	Temperature difference from room temperature, °C
TFF	Tangential flow filtration
V_{media}	Volume of culture media, L
$V_{perfusion}$	Culture volume for perfusion culture, L
$V_{working}$	Working volume of the culture, L
$V_{0,perfusion}$	Initial culture volume for perfusion culture, L
$w_{desire,p}$	Desired amount of API p per year, µg yr^{-1}
X_{batch}	Concentration of viable cells for batch culture, cell mL^{-1}
$X_{perfusion}$	Concentration of viable cells for perfusion culture, cell mL^{-1}
$X_{0,batch}$	Initial concentration of viable cells for batch culture, cell mL^{-1}
$X_{0,perfusion}$	Initial concentration of viable cells for perfusion culture, cell mL^{-1}

Greek Letters

θ	Perturbation range, –
μ_{batch}	Specific growth rate for batch culture, hr^{-1}
$\mu_{perfusion}$	Specific growth rate for perfusion culture, hr^{-1}
$\mu_{max,batch}$	Maximum specific growth rate for batch culture, hr^{-1}
$\mu_{max,perfusion}$	Maximum specific growth rate for perfusion culture, hr^{-1}
$\mu_{solution}$	Viscosity of the solution, Pa s
$\rho_{solution}$	Density of the solution, kg m^{-3}

References

Ahn, W.S., Antoniewicz, M.R., 2011. Metabolic flux analysis of CHO cells at growth and non-growth phases using isotopic tracers and mass spectrometry. Metab. Eng. 13, 598–609. https://doi.org/10.1016/j.ymben.2011.07.002

Badsha, M.B., Kurata, H., Onitsuka, M., Oga, T., Omasa, T., 2015. Metabolic analysis of antibody producing Chinese hamster ovary cell culture under different stresses conditions. J. Biosci. Bioeng. 122, 117–124. https://doi.org/10.1016/j.jbiosc.2015.12.013

Bielser, J.M., Wolf, M., Souquet, J., Broly, H., Morbidelli, M., 2018. Perfusion mammalian cell culture for recombinant protein manufacturing – A critical review. Biotechnol. Adv. 36, 1328–1340. https://doi.org/10.1016/j.biotechadv.2018.04.011

Bunnak, P., Allmendinger, R., Ramasamy, S. V., Lettieri, P., Titchener-Hooker, N.J., 2016. Life-cycle and cost of goods assessment of fed-batch and perfusion-based manufacturing processes for mAbs. Biotechnol. Prog. 32, 1324–1335. https://doi.org/10.1002/btpr.2323

Clincke, M.F., Moelleryd, C., Zhang, Y., Lindskog, E., Walsh, K., Chotteau, V., 2013a. Very high density of CHO cells in perfusion by ATF or TFF in WAVE bioreactor™: Part I: Effect of the cell density on the process. Biotechnol. Prog. 29, 754–767. https://doi.org/10.1002/btpr.1704

Clincke, M.F., Mölleryd, C., Samani, P.K., Lindskog, E., Fäldt, E., Walsh, K., Chotteau, V., 2013b. Very high density of Chinese hamster ovary cells in perfusion by alternating tangential flow or tangential flow filtration in WAVE bioreactor™-part II: Applications for antibody production and cryopreservation. Biotechnol. Prog. 29, 768–777. https://doi.org/10.1002/btpr.1703

Dowd, J.E., Jubb, A., Kwok, K.E., Piret, J.M., 2003. Optimization and control of perfusion cultures using a viable cell probe and cell specific perfusion rates. Cytotechnology 42, 35–45. https://doi.org/10.1023/A:1026192228471

Ecker, D.M., Jones, S.D., Levine, H.L., 2015. The therapeutic monoclonal antibody market. MAbs 7, 9–14. https://doi.org/10.4161/19420862.2015.989042

Fisher, A.C., Kamga, M.-H., Agarabi, C., Brorson, K., Keem S.L., Yoon, S., 2019, The current scientific and regulatory landscape in advancing integrated continuous biopharmaceutical manufacturing, Trends Biotechnol. 37, 253–267. https://doi.org/10.1016/j.tibtech.2018.08.008

Fox, S.R., Patel, U.A., Yap, M.G.S., Wang, D.I.C., 2004. Maximizing interferon-γ production by chinese hamster ovary cells through temperature shift optimization:Experimental and modeling. Biotechnol. Bioeng. 85, 177–184. https://doi.org/10.1002/bit.10861

Galleguillos, S.N., Ruckerbauer, D., Gerstl, M.P., Borth, N., Hanscho, M., Zanghellini, J., 2017. What can mathematical modelling say about CHO metabolism and protein glycosylation? Comput. Struct. Biotechnol. J. 15, 212–221. https://doi.org/10.1016/j.csbj.2017.01.005

Hiller, G.W., Ovalle, A.M., Gagnon, M.P., Curran, M.L., Wang, W., 2017. Cell-controlled hybrid perfusion fed-batch CHO cell process provides significant productivity improvement over conventional fed-batch cultures. Biotechnol. Bioeng. 114, 1438–1447. https://doi.org/10.1002/bit.26259

Hu, S., Deng, L., Wang, H., Zhuang, Y., Chu, J., Zhang, S., Li, Z., Guo, M., 2011. Bioprocess development for the production of mouse-human chimeric anti-epidermal growth factor receptor vIII antibody C12 by suspension culture of recombinant Chinese hamster ovary cells. Cytotechnology 63, 247–258. https://doi.org/10.1007/s10616-011-9336-y

Huang, Y.M., Hu, W.W., Rustandi, E., Chang, K., Yusuf-Makagiansar, H., Ryll, T., 2010. Maximizing productivity of CHO cell-based fed-batch culture using chemically defined media conditions and typical manufacturing equipment. Biotechnol. Prog. 26, 1400–1410. https://doi.org/10.1002/btpr.436

Karst, D.J., Scibona, E., Serra, E., Bielser, J.M., Souquet, J., Stettler, M., Broly, H., Soos, M., Morbidelli, M., Villiger, T.K., 2017a. Modulation and modeling of monoclonal antibody N-linked glycosylation in mammalian cell perfusion reactors. Biotechnol. Bioeng. 114, 1978–1990. https://doi.org/10.1002/bit.26315

Karst, D.J., Serra, E., Villiger, T.K., Soos, M., Morbidelli, M., 2016. Characterization and comparison of ATF and TFF in stirred bioreactors for continuous mammalian cell culture processes. Biochem. Eng. J. 110, 17–26. https://doi.org/10.1016/j.bej.2016.02.003

Karst, D.J., Steinebach, F., Soos, M., Morbidelli, M., 2017b. Process performance and product quality in an integrated continuous antibody production process. Biotechnol. Bioeng. 114, 298–307. https://doi.org/10.1002/bit.26069

Kelly, P.S., McSweeney, S., Coleman, O., Carillo, S., Henry, M., Chandran, D., Kellett, A., Bones, J., Clynes, M., Meleady, P., Barron, N., 2016. Process-relevant concentrations of the leachable bDtBPP impact negatively on CHO cell production characteristics. Biotechnol. Prog. 32, 1547–1558. https://doi.org/10.1002/btpr.2345

Kiparissides, A., Pistikopoulos, E.N., Mantalaris, A., 2015. On the model-based optimization of

secreting mammalian cell (GS-NS0) cultures. Biotechnol. Bioeng. 112, 536–548. https://doi.org/10.1002/bit.25457

Klutz, S., Holtmann, L., Lobedann, M., Schembecker, G., 2016. Cost evaluation of antibody production processes in different operation modes. Chem. Eng. Sci. 141, 63–74. https://doi.org/10.1016/j.ces.2015.10.029

Kumar, N., Gammell, P., Clynes, M., 2007, Proliferation control strategies to improve productivity and survival during CHO based production culture, Cytotechnology 53, 33–46. https://doi.org/10.1007/s10616-007-9047-6

Langer, E.S., Rader, R.A., 2014. Continuous Bioprocessing and Perfusion: Wider Adoption Coming as Bioprocessing Matures. Bioprocess. J. 13, 43–49.

Lee, J.C., Chang, H.N., Oh, D.J., 2005. Recombinant Antibody Production by Perfusion Cultures of rCHO Cells in a Depth Filter Perfusion System. Biotechnol. Prog. 21, 134–139. https://doi.org/10.1021/bp0497942

Li, G, Rabitz, H., Yelvington, P.E., Oluwole, O.O., Bacon, F., Kolb, C.E., Schoendorf, J., 2010, Global Sensitivity Analysis for Systems with Independent and/or Correlated Inputs, *J. Phys. Chem. A*, 114, 6022–6032. https://doi.org/10.1021/jp9096919

Masterton, R.J., Smales, C.M., 2014. The impact of process temperature on mammalian cell lines and the implications for the production of recombinant proteins in CHO cells. Pharm. Bioprocess. 2, 49–61. https://doi.org/10.4155/PBP.14.3

Meager, A., Gaines Das, R., Zoon, K., Mire-Sluis, A., 2001. Establishment of new and replacement World Health Organization International Biological Standards for human interferon alpha and omega. J. Immunol. Methods 257, 17–33. https://doi.org/10.1016/S0022-1759(01)00460-4

Mears, L., Stocks, S.M., Albaek, M.O., Sin, G., Gernaey, K. V., 2017. Application of a mechanistic model as a tool for on-line monitoring of pilot scale filamentous fungal fermentation processes—The importance of evaporation effects. Biotechnol. Bioeng. 114, 589–599. https://doi.org/10.1002/bit.26187

Morris, M.D., 1991, Factorial Sampling Plans for Preliminary Computational Experiments, Technometrics, 33, 161–174. https://doi.org/10.2307/1269043

Otto, R., Santagostino, A., Schrader, U., 2014. The beauty and the beast: A perspective on biopharmaceuticals. McKinsey&Company 9–18.

Pollock, J., Coffman, J., Ho, S. V., Farid, S.S., 2017. Integrated continuous bioprocessing: Economic, operational, and environmental feasibility for clinical and commercial antibody manufacture. Biotechnol. Prog. 33, 854–866. https://doi.org/10.1002/btpr.2492

Quiepo, N.V., Haftka, R.T., Shyy, W., Goel, T., Vaidyanathan, R., Tucker, P.K., 2005, Surrogate-based analysis and optimization, Prog. Aerosp. Sci., 41, 1–28. https://doi.org/10.1016/j.paerosci.2005.02.001

Rocha, M., Mendes, R., Rocha, O., Rocha, I., Ferreira, E.C., 2014. Optimization of fed-batch fermentation processes with bio-inspired algorithms. Expert Syst. Appl. 41, 2186–2195. https://doi.org/10.1016/j.eswa.2013.09.017

Rodman, A.D., Fraga, E.S., Gerogiorgis, D., 2018. On the application of a nature-inspired stochastic evolutionary algorithm to constrained multi-objective beer fermentation optimisation. Comput. Chem. Eng. 108, 448–459. https://doi.org/10.1016/j.compchemeng.2017.10.019

Rodman, A.D., Gerogiorgis, D.I., 2017. Dynamic optimization of beer fermentation: Sensitivity analysis of attainable performance vs. product flavour constraints. Comput. Chem. Eng. 106, 582–595. https://doi.org/10.1016/j.compchemeng.2017.06.024

Rodman, A.D., Gerogiorgis, D.I., 2016. Multi-objective process optimisation of beer fermentation via dynamic simulation. Food Bioprod. Process. 100, 255–274.

https://doi.org/10.1016/j.fbp.2016.04.002

Rouiller, Y., Bielser, J.M., Brühlmann, D., Jordan, M., Broly, H., Stettler, M., 2016. Screening and assessment of performance and molecule quality attributes of industrial cell lines across different fed-batch systems. Biotechnol. Prog. 32, 160–170. https://doi.org/10.1002/btpr.2186

Saltelli, A., Ratto, M., Tarantola, S., Campolongo, F., 2005, Sensitivity analysis for chemical modes, Chem. Rev., 105, 2811–2827. https://doi.org/10.1021/cr040659d

Schaber, S.D., Gerogiorgis, D.I., Ramachandran, R., Evans, J.M.B., Barton, P.I., Trout, B.L., 2011. Economic Analysis of Integrated Continuous and Batch Pharmaceutical Manufacturing: A Case Study. Ind. Eng. Chem. Res. 50, 10083–10092. https://doi.org/10.1021/ie2006752

Shakibaie, M., Tabandeh, F., Zomorodipour, A.R., Mohammad-beigi, H., Ebrahimi, S., Habib-ghomi, H., 2011. Kinetics, Experimental and Simulation Studies of Chinese Hamster Ovary Cell Growth in a Packed-Bed Bioreactor. Biotechnology 15, 1568–1575.

Sobol, I.M., 2001, Global sensitivity indices for nonlinear mathematical models and their Monte Carlo estimates, Math. Comput. Simul., 55, 271–280. https://doi.org/10.1016/S0378-4754(00)00270-6

Sokolov, M., Ritscher, J., MacKinnon, N., Bielser, J.M., Brühlmann, D., Rothenhäusler, D., Thanei, G., Soos, M., Stettler, M., Souquet, J., Broly, H., Morbidelli, M., Butté, A., 2017. Robust factor selection in early cell culture process development for the production of a biosimilar monoclonal antibody. Biotechnol. Prog. 33, 181–191. https://doi.org/10.1002/btpr.2374

Spann, R., Roca, C., Kold, D., Eliasson Lantz, A., Gernaey, K. V., Sin, G., 2018. A probabilistic model-based soft sensor to monitor lactic acid bacteria fermentations. Biochem. Eng. J. 135, 49–60. https://doi.org/10.1016/j.bej.2018.03.016

Steinebach, F., Ulmer, N., Wolf, M., Decker, L., Schneider, V., Wälchli, R., Karst, D., Souquet, J., Morbidelli, M., 2017. Design and operation of a continuous integrated monoclonal antibody production process. Biotechnol. Prog. 33, 1303–1313. https://doi.org/10.1002/btpr.2522

Sunley, K., Tharmalingam, T., Butler, M., 2008. CHO cells adapted to hypothermic growth produce high yields of recombinant β-interferon. Biotechnol. Prog. 24, 898–906. https://doi.org/10.1002/btpr.9

Templeton, N., Dean, J., Reddy, P., Young, J.D., 2013. Peak antibody production is associated with increased oxidative metabolism in an industrially relevant fed-batch CHO cell culture. Biotechnol. Bioeng. 110, 2013–2024. https://doi.org/10.1002/bit.24858

Tharmalingam, T., Sunley, K., Butler, M., 2008. High yields of monomeric recombinant β-interferon from macroporous microcarrier cultures under Hypothermic Conditions. Biotechnol. Prog. 24, 832–838. https://doi.org/10.1002/btpr.8

Vergara, M., Becerra, S., Berrios, J., Osses, N., Reyes, J., Rodríguez-Moyá, M., Gonzalez, R., Altamirano, C., 2014, Differential effect of culture temperature and specific growth rate on CHO cell behavior in chemostat culture, PLoS One 9: e93865.

Xing, Z., Bishop, N., Leister, K., Li, Z.J., 2010. Modeling kinetics of a large-scale fed-batch CHO cell culture by markov chain monte carlo method. Biotechnol. Prog. 26, 208–219. https://doi.org/10.1002/btpr.284

Xing, Z., Kenty, B.M., Li, Z.J., Lee, S.S., 2009. Scale-up analysis for a CHO cell culture process in large-scale bioreactors. Biotechnol. Bioeng. 103, 733–746. https://doi.org/10.1002/bit.22287

Yang, W.C., Minkler, D.F., Kshirsagar, R., Ryll, T., Huang, Y.M., 2016. Concentrated fed-batch cell culture increases manufacturing capacity without additional volumetric capacity. J. Biotechnol. 217, 1–11. https://doi.org/10.1016/j.jbiotec.2015.10.009

Yoon, S.K., Kim, S.H., Lee, G.M., 2003. Effect of low culture temperature on specific productivity and transcription level of anti-4-1BB antibody in recombinant Chinese hamster ovary cells.

Biotechnol. Prog. 19, 1383–1386. https://doi.org/10.1021/bp034051m

Zhang, Y., Stobbe, P., Silvander, C.O., Chotteau, V., 2015. Very high cell density perfusion of CHO cells anchored in a non-woven matrix-based bioreactor. J. Biotechnol. 213, 28–41. https://doi.org/10.1016/j.jbiotec.2015.07.006